High-Pressure Plastic Deformation of Lead Metasilicate Glass Accessed by Raman Spectroscopy: Insights into the Q n distribution

R. B. Pena, V Laurent, T Deschamps, E Romeo, A. Picinin, Christine Martinet, P Pizani

High-Pressure Plastic Deformation of Lead Metasilicate Glass Accessed by Raman Spectroscopy: Insights into the Q^n distribution

R.B. Pena[a,b,c*]; V. Laurent[a]; T. Deschamps[a]; E Romeo[a]; A. Picinin[b,c] ; C. Martinet[a]; P.S. Pizani[b,c]

[a] Institut Lumière Matière (ILM), UMR5306 Université Lyon 1 - CNRS, Université de Lyon 69622 Villeurbanne, France.

[b] Federal University of São Carlos, Physics Department, 13565 - 905 São Carlos, SP, Brazil.

[c] Department of Materials Engineering, Center for Research, Technology and Education in Vitreous Materials, Federal University of São Carlos, 13565-905, São Carlos, SP, Brazil.

*Corresponding author e-mail: rafaellabartz@gmail.com

Highlights

- Raman investigation of cold densified $PbSiO_3$ glass up to 23 GPa
- Analysis of high-frequency band by the barycenter and Q^n curve fit were done
- The elastic limit is estimated at 4 GPa, well below other silicate glasses
- Hydrostatic pressure in the plastic regime induces silica network depolymerization.

Abstract

In this study, lead metasilicate glasses ($PbSiO_3$) were densified at different maximum pressures in a diamond anvil cell (DAC) at room temperature. The densified glass samples were investigated ex-situ by Raman spectroscopy to probe their pressure-induced plastic deformation limit and permanent structural modifications on the Q^n distribution. With a high Pb content, this glass exhibits a low elastic limit at ~4 GPa, which is linked to an initial compact structure. Spectral curve fitting of the high-frequency region of the Raman spectra, consisting of symmetric Si-O stretching modes, exhibit subtle Q^n population modifications with maximum pressure. This reveals silica network depolymerization where the proportion of non-bridging oxygens (NBO) increases at the expense of bridging oxygens (BO). Possible densification mechanisms are discussed in contrast to those known in other silicate glasses.

Keywords: *Lead Metasilicate Glass; High-Pressure; Structure; Densification; Raman Spectroscopy; Medium-Range Order.*

1. Introduction

Lead silicate glasses are widely used in different commercial applications [1] due mostly to their high refractive index, and X- and γ-ray attenuation [2, 3], which are closely linked to their high density. It is well known that the $PbO\text{-}SiO_2$ system can form glasses over a wide compositional range, up to 96 mol.% PbO [4]. Because of the excellent glass-forming ability of these glasses and melts, they have been the focus of a numerous structural studies at ambient pressure: X-ray and/or neutron diffraction [5-11]; Raman spectroscopy [12-20]; infrared spectroscopy [13-15, 18, 21, 22]; nuclear magnetic resonance (NMR) [10, 18, 23-29]; molecular dynamics (MD) [20, 30-33]; X-ray absorption near edge structure (XANES) [24]; extended X-ray absorption fine structure (EXAFS) [33, 34]; X-ray photoelectron spectroscopy (XPS) [35-38].

Many of these studies attempt to describe the role played by lead atoms in the glass network. Usually lead cations are assigned as either modifier or intermediate cation, depending on the lead content. Nevertheless, there is no consensus in the literature for the precise composition where this transition in the role of lead occurs.

To the best of our knowledge, the only reported experimental study on the $PbO\text{-}SiO_2$ glass under high-pressure was conducted via hot-compression by Yoshimoto *et al.*[39], for compositions ranging from 33 to 67 mol.% PbO. These authors focused on mechanical properties, reporting an increase in the hardness and Young's modulus. While the densification rates decreased monotonically as a function of the lead content, the Young's modulus and hardness were reported to display a minimum at the metasilicate composition.

In this context, our investigation will provide new insights about the structural modifications driven by the densification of lead metasilicate glass. Description of the polymerization state in silicate glasses is often based on the Q^n distribution [40]. The Q^n ('quaternary') species refer to the connectivity of SiO_4 tetrahedra within the silicate network, where n ranges from 0 to 4 bridging oxygens per tetrahedron (Figure 1).

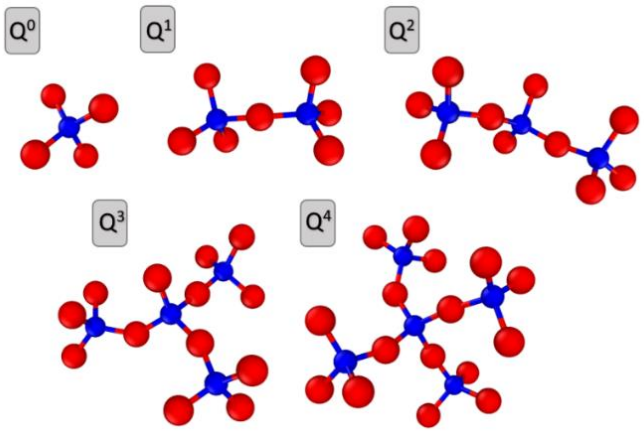

Figure 1: The Q^n units are related to the (SiO_4) tetrahedra connectivity within the glass network, where n ranges from 0 to 4 bridging oxygens per tetrahedron.

At room temperature conditions, the Q^n distribution in lead metasilicate glasses has been well studied by molecular dynamics simulations [20, 30], nuclear magnetic resonance [18, 23, 28], and Raman spectroscopy [19, 20]. From all of the reported studies, the structure of these glasses contains mostly Q^2 tetrahedra. The lead metasilicate composition has been studied as a function of the temperature, which revealed new details on the crystallization pathways [41] and glass structure [20]. The corroborating results between Raman spectroscopy and molecular dynamics proposed a curve fit model based on two distinct Q^3 species [20]. These species, Q^3 and $Q^{3'}$, were associated with a bimodal distribution displayed by the Pb-Si pair correlation function. This curve fit model agrees with the Q^2 and Q^3 proportions determined by NMR at room temperature as well the Q^n distribution derived from molecular dynamics simulations at high temperatures. We aim to extend this Raman curve fit model to the densified glass.

In this work, we analyze ex-situ lead metasilicate glass samples compressed to different maximum pressures at room temperature using a diamond anvil cell (DAC). This study was performed in order to characterize the hydrostatic pressure effects above the elastic limit and relate them to the structural modifications indicated by the Q^n population changes.

2. Methods

2.1 *Glass preparation*

The $PbSiO_3$ (PS) glass was prepared by standard splat quench method in 100 g batch made from ground SiO_2 (Vitrovita, Brazil) and Pb_3O_4 (Sigma-Aldrich, USA). The specimens are from the same batch as in these works [20, 41-43]. Electron probe microanalysis (EPMA) indicates an accurate composition, within 0.5 mol.%, of lead metasilicate as reported [41].

A series of PS pieces from this batch were compressed to different maximum pressures in a Chervin-type DAC. Stainless-steel gaskets were indented and drilled, resulting in chambers with a ~50 μm height and 200 μm diameter. In each run, the DAC chamber was filled with PS samples, ruby chips as a pressure sensor, and a 4:1 methanol-ethanol mixture as the pressure-transmitting medium. This alcohol solution has been reported to remain hydrostatic up to 10.5 GPa and is quasi-hydrostatic above [44]. The R1 ruby fluorescence line of Cr^{3+} excited with a 633 nm laser enabled the pressure determination in-situ [45]. Eight distinct PS glass pieces were compressed to the following maximum pressures: 4.1 GPa; 5.7 GPa; 9.9 GPa; 12.6 GPa; 14.3 GPa; 15.5 GPa; 20 GPa and 23 GPa. The pressure errors inside the DAC were estimated to be ±0.1 GPa within the hydrostatic pressure region, ±0.5 GPa up to 16 GPa, and ±1 GPa above 16 GPa.

2.2 Raman measurements and spectral analysis

Raman measurements were taken using a LabRAM Aramis micro-Raman spectrometer from Horiba Jobin Yvon. The 473 nm laser wavelength was used as an excitation source and the scattered light was collected by a 50x long working-distance objective. The Raman spectra were collected for each of the densified PS glass samples using the 1800 slits/mm grating between 600 and 1300 cm^{-1}. Each spectrum is an average of five measurements of 300 seconds of accumulation time.

All analyses were carried out considering the high-frequency region of the Raman spectra, which was baseline corrected by a cubic function fit by selecting the flat spectral region that precedes and follows the envelope range.

The barycenter as a function of maximum pressure was determined by integrating and normalizing the intensity data from 790 to 1200 cm^{-1} (envelope range), and subsequently calculating the frequency that separates the envelope into two parts of equal area, as described here [46].

The Q^n population as a function of the maximum pressure was obtained by applying the curve fit model of Sampaio *et al.* [20]. Data were fit using the software Fityk (version 0.9.8) then applying the Nelder-Mead Simplex fitting algorithm. The Q^n analysis was performed by systematically adjusting or holding constant the peak centers and widths.

3. Results and Discussions

Figure 2 shows the high-frequency part of the spectra of densified PS glasses, due to the symmetric Si-O stretching vibrations [20]. The Raman spectra show a broad envelope, which shifts to lower wavenumbers with increasing pressure. No new peaks are observed as a result of the plastic compression/decompression cycle. Similar results using infrared spectroscopy were reported on 2.6% densified PS glasses released from 6 GPa and ~230 ºC [39].

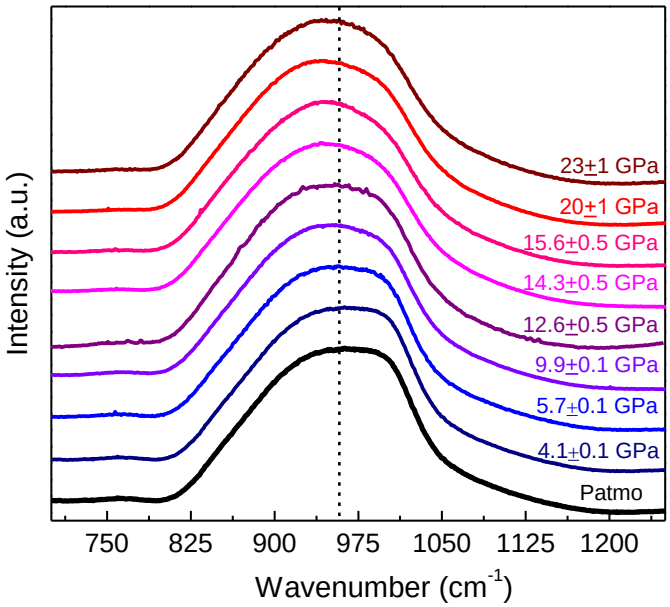

Figure 2: High-frequency (800-1200 cm^{-1}) Raman spectra of permanently densified $PbO.SiO_2$ samples were recorded at atmospheric pressure after hydrostatic compression in the DAC at room temperature. The indicated pressures correspond to the maximum pressure. The dashed line marks the barycenter at atmospheric pressure.

Our discussion is divided into two parts, the first addresses the high-frequency envelope shift described by the barycenter (χ_b), whereas the second part describes the curve fit modelling of the Q^n species. The barycenter reveals the overall structural modifications resulting from densification and provides an estimation of the elastic limit. The latter part depicts the pressure-induced depolymerization producing non-bridging oxygens (NBO).

3.1. Elastic Limit

At first glance, we assess the evolution of the high-frequency Raman envelope by determining their barycenter (χ_b). The χ_b reflects the simultaneous evolution of the envelope shape and offset of the peak maxima [47]. The χ_b behavior unveils two important trends for the densified PS samples (Figure 3). For uncompressed PS glass (P_{atmo}), χ_b is 958 cm^{-1} and remains invariant for the sample recovered up to ~4 GPa. Above 4 GPa, the compression induces a progressive decrease in χ_b, where plastic deformation starts to take place. The shift in χ_b stops at 950 cm^{-1} around 20 GPa. The χ_b shifts toward lower frequencies along with a subtle change in the envelope shape is an indication of depolymerization as the more polymerized Q^n species would shift χ_b to the higher frequencies [19, 20].

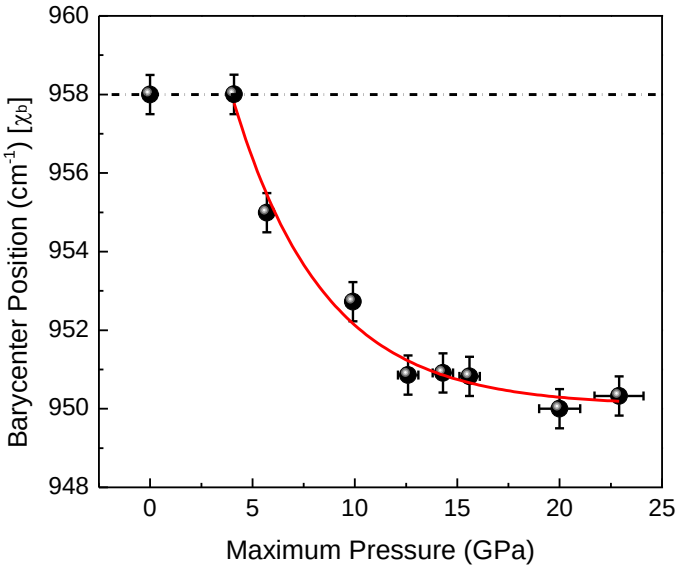

Figure 3: Barycenter of the high-frequency Raman region as a function of the maximum pressure. An exponential decay function (red line) fits the experimental points (black circles), while a horizontal line marks the uncompressed value, reversible part.

The elastic limit corresponds to the maximum pressure below which the system can recover its initial state once returned to ambient conditions; i.e., where elastic deformation ceases. Above this elastic limit, irreversible structural modifications and permanent densification occur. The χ_b behavior indicates that the elastic limit of the lead metasilicate glass is about 4 GPa (Figure 3). It is worth noting that this limit is low when compared to vitreous silica [48-53] and other silicate glasses [54-56].

Regarding vitreous silica, its elastic limit is ~9 GPa, under hydrostatic conditions at room temperature [48-53, 57]. In the elastic regime, the in-situ compaction mechanism involves a narrowing of the inter-tetrahedral (Si-O-Si) angle [51, 52, 57], in such a way that the short-

range order remains preserved. There are no significant changes in the Si-O bond distances and tetrahedral O-Si-O angles [57]. Meanwhile, as the pressure increases into the plastic regime, the coordination gradually changes, from ^{IV}Si to ^{V}Si, and then to ^{VI}Si. The exact pressures where these transformations take place is not clearly established in the literature [52, 57-61].

Above 9 GPa, the retrieved vitreous silica shows permanent densification [50], with a densification rate that varies gradually with maximum pressure, reaching up to 21% at 25 GPa [48-53]. The densified glass recovers its short-range order original features (^{IV}Si coordination, tetrahedral O-Si-O angle distribution [57]). However, modifications in the medium-range order of silica glass do show a decrease in the Si-O-Si angle distribution [62] reducing the Si-Si distances by decreasing the void space. In multicomponent MO-silicate glasses, the permanent structural modifications have further been associated with the formation of highly coordinated M and/or Si cations, and sometimes with polymerization of the Q^n species [54, 63-71].

Yoshimoto *et al.* [39] hot-densified lead silicate glasses of different compositions at fixed conditions (6 GPa and $0.75*T_g$) and observed a decrease in the densification rate with the increasing PbO content. The authors argue that this behavior is linked to the difficulty in accommodating large Pb^{2+} ions into the atomic scale voids within the silica glass network. This argument is consistent with the decrease in the inter-tetrahedral (Si-O-Si) angle playing an important role in the densification mechanism, and to the progressive decrease in the elastic limit at higher lead contents; as observed from vitreous silica to PS glass.

In contrast to vitreous silica, the PS glass exhibits a more compact and depolymerized structure. Kohara *et al.* [11] estimated that the total volume occupied by the voids in vitreous silica is 31.9%, while in PS glasses it amounts to 11.3%. A fact that supports its low elastic limit. While vitreous silica presents ideally a completely polymerized, Q^4 structure, the PS structure contains mostly Q^2 tetrahedra [18-20, 23, 28, 30], with a great number of NBOs. Further complexity might arise from the contribution of lead cations, which in PS start to form their own network. In PS glass, some lead cations act as modifiers while a small portion might play the role of network formers.

Structural correlation to other silicate systems is not straightforward. In soda-lime silicate glass, containing SiO_2 (72 mol.%), Na_2O (15 mol.%) and CaO (8 mol.%), the elastic limit lies around 7 GPa as above this pressure, an increase of Q^2 at the expense of Q^3 tetrahedra has been observed [54]. Under hydrostatic pressure, a glass composed of SiO_2 (80 wt.%), CaO (6 wt.%), MgO (5 wt.%) and Na_2O (5 wt.%) shows irreversible compaction beyond 8 GPa [55]. In a nominal $Mg_3Al_2Si_3O_{12}$ glass, the elastic limit was determined to be 6 GPa. Above this pressure, Al coordination number increases, whereas the presence of highly coordinated Si species is

negligible [56]. Therefore, to our knowledge, PS glass shows the lowest elastic limit likely due to its dense packing and low void space.

3.2. Pressure-Induced Structural Modifications: Q^n population and non-bridging oxygens

For pressures above the elastic limit, the high-frequency envelope changes with the maximum pressure (Figure 2), and shift towards lower wavenumbers. The curve fit of this broadband without well-defined peaks is a model-dependent procedure. The Q^n population evaluation is given by normalizing the area under the spectrum, then fitting a series of functions to model the distinct Q^n vibrational modes.

Sampaio *et al.* [20] curve fit model well describes the Q^n population for the PS glass structure. This model was structurally consistent with molecular dynamics simulations and fits the high-frequency Raman envelope using six Gaussian components corresponding to Q^0, Q^1, Q^2, Q^3, $Q^{3'}$ and Q^4 contributions (Figure 4a). The distinct Q^3 species, Q^3 and $Q^{3'}$, are associated with the Pb-Si pair correlation function which displays a bimodal distribution [20] related to longer or shorter bridging distances between the NBO and the lead cations.

In order to quantify the Q^n species as a function of densification, we assume no new peaks should be added as none are observed in the spectra (Figure 2) and that the relative cross-sections for the Raman scattering do not change for the compressed samples. Sampaio's model is based on the curve fit of the high-frequency envelope into Gaussian functions, but it could be revised by incorporating new developments using mixed Gaussian and Lorentzian line shapes [72-74]. For the lead metasilicate composition, the full set of Q^n line shapes were considered to be Gaussian because of the high lead content and the broader Si-O-Si angle distribution of this glass relative to vitreous silica [20, 30].

Table 1: Center position and FWHM parameters determined by Sampaio et al.[20] for the curve fit of PS high-frequency Raman spectra at room temperature.

	Center Position (cm^{-1})	**FWHM (cm^{-1})**
Q^0	847	54
Q^1	897	73
Q^2	955	78
Q^3	1001	53
$Q^{3'}$	1043	79
Q^4	1103	103

The Gaussian parameters determined by Sampaio *et al.* [20] at room temperature are presented in Table 1. For each of the analyses, this set is used as initial values, holding the center position and full width at half maximum (FWHM) either as a constant or as a variable. Where left variable, the peak center was constrained to $\Delta\nu = \pm 2$ cm^{-1} per pressure, and the ΔFWHM was constrained to ± 0.2 cm^{-1}. These parameters may affect the area under a given Gaussian component, directly as the width may vary, or indirectly as the center position varies, once the spectral intensity is a function of the wavenumber. For clarity, each fitting procedure is listed in Table 2, where, for example, the P1 procedure uses constant parameters, whereas procedure P4 allowed both to vary from pressure to pressure.

Table 2: Distinct procedures applied for performing the high-frequency band curve fit holding the center position and full width at half maximum (FWHM) either as a constant or as a variable.

	Center Position	**FWHM**
P1	Constant	Constant
P2	Variable	Constant
P3	Constant	Variable
P4	Variable	Variable

Figure 4 illustrates the contribution of each of the altered Gaussian parameters over the total Q^n quantification. Comparing the outcomes of each procedure, we note that the P2 procedure shows deviations in the estimation of Q^4, whereas the P3 procedure underestimates the Q^2 population and, further, delivers worse agreement with the Q^1 and Q^0 population. The P1 and P4 procedures display the same trends, where both the Q^0 and Q^1 populations increase slightly whereas Q^4 decreases modestly and Q^2 remains about the same. More interestingly, as the maximum pressure increases, the $Q^{3'}$ is favored over the Q^3 units and their total population (Q^3_{tot}) decreases. Due to their link with the Pb-Si pair correlation function, the P1 and P4 results suggest that pressure brings Pb closer to Si by converting part of the Q^3 to $Q^{3'}$ units.

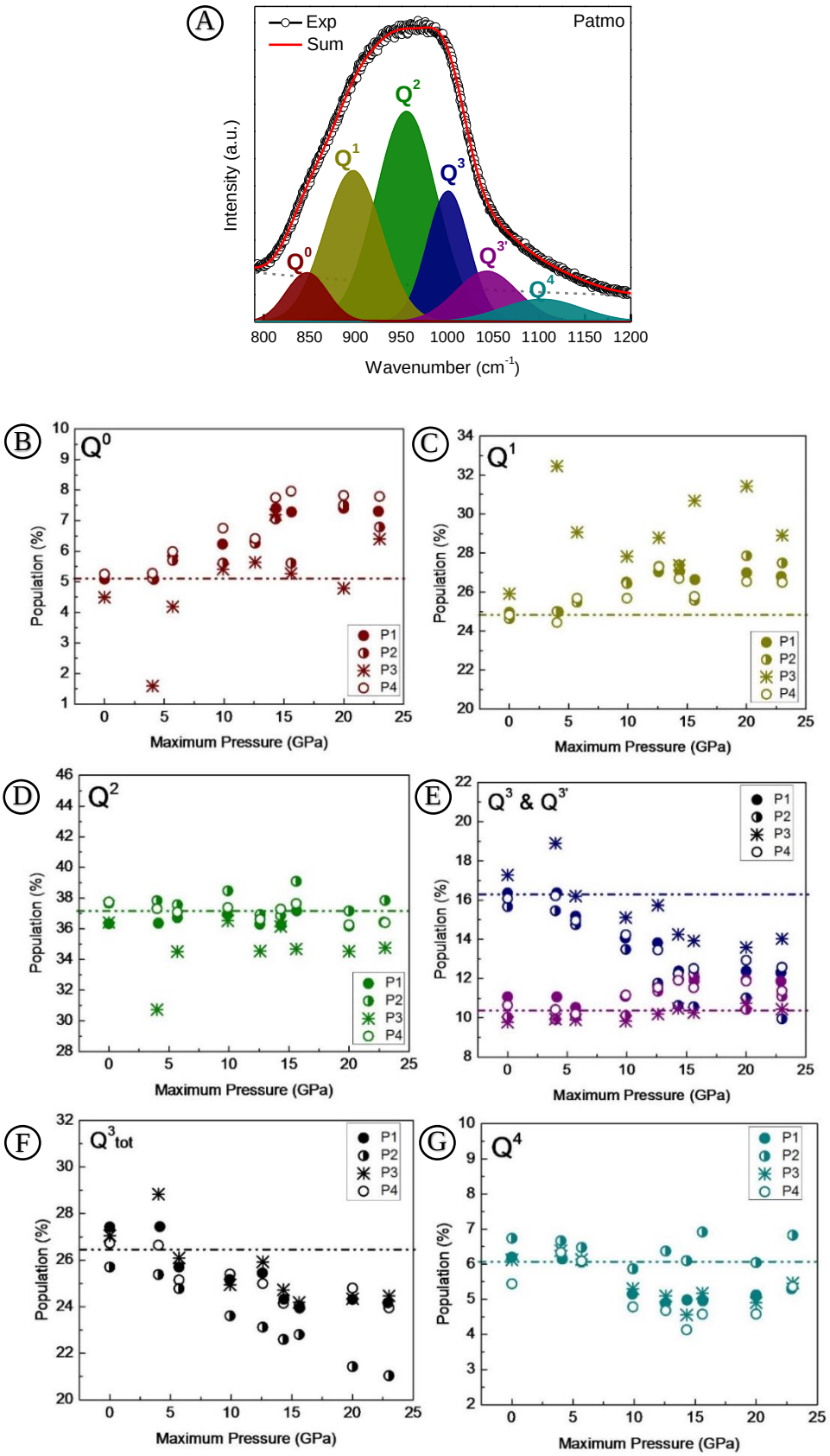

Figure 4: (a) Q^n population curve fit of the uncompressed PS glass (Patmo) and the evolution of (b) Q^0; (c) Q^1; (d) Q^2;(e) Q^3 and Q3'; (f) Q^3tot and (g) Q^4 as a function of the maximum pressure obtained using the four distinct procedures (Table 2). The horizontal lines mark the population average for each Q^n in PS- Patmo. Uncertainty in the Q^n population evaluation is estimated as ± 1% (not shown).

Some studies on alkaline [63, 65] and alkaline-earth [66, 67] silicates under high-pressure show that the Q^n distribution follows the disproportionation reaction:

$$2Q^n \rightarrow Q^{n+1} + Q^{n-1} \quad (1)$$

This equation predicts that the consumption of two given Q^n tetrahedra produces one immediately more polymerized (Q^{n+1}) and the other less polymerized (Q^{n-1}) tetrahedra. From our curve-fit results shown in Fig.4, we have applied Eq. (1) to observe the Q^n evolution. In the case of PS one may expect the disproportionation reaction $2Q^2 \rightarrow Q^3_{tot} + Q^1$, however, our curve-fit procedures are unanimous in showing no appreciable variation in the Q^2 population. It is important to note that we observe a trend, although subtle, in the depolymerization where Q^4 and Q^3_{tot} are ultimately converted to produce more Q^1 and Q^0 species. It follows that the simple forms of Eq. (1) does not hold in describing the Q^n population modifications driven by pressure to the PS composition.

This depolymerization can be described by equilibria of the oxygen species [38] by:

$$BO + O^{2-} \leftrightarrow 2NBO \quad (2)$$

Where a "bridging oxygen" (BO) is an oxygen bonded to two silicon cations (i.e., Si-O-Si), therefore linking the silicate lattice. On the other hand, a "non-bridging oxygen" (NBO) bonds one silicon cation to a lead cation that plays the role of modifier (i.e., Si-O-Pb). A "free oxygen" (O^{2-}), is *not* bonded to silicon but links lead cations together (i.e., Pb-O-Pb), potentially connecting the lead network sub-lattice. O^{2-} is also referred to as metal-bridging oxygen or non-network oxygen and has been reported in metasilicate compositions [20, 29, 30, 37].

Detailed information regarding the O^{2-} units is not directly accessible from Raman spectroscopy data [14]. Thus, the BO and NBO contents were extrapolated based on the assumption that these are the only oxygen species in the glass, the same procedure was explicitly adopted there, to the NaO-SiO_2 glass system investigated by ^{29}Si NMR spectroscopy [75]. The NBO content can be rough determined from the Q^n population:

$$NBO = 4Q^0 + 3Q^1 + 2Q^2 + Q^3_{tot} \quad (3)$$

And the BO content as well:

$$BO = \frac{1}{2}(Q^1 + 2Q^2 + 3Q^3_{tot} + 4Q^4) \quad (4)$$

Where Q^3_{tot} is the sum of the two distinct Q^3 and $Q^{3'}$ units. This treatment gives a picture of the silicate lattice, providing BO and NBO proportions between them. Evaluation of PS at room-condition indicates a 2% O^{2-} content in the uncompressed glass [29].

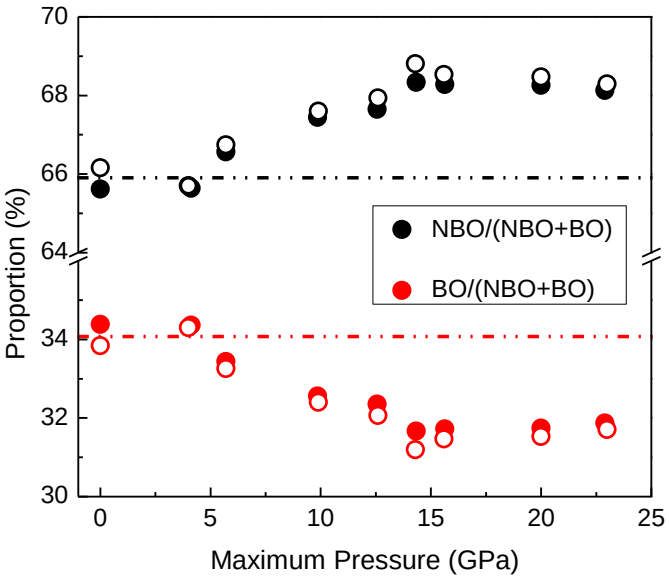

Figure 5: Bridging oxygen ($\frac{BO}{NBO+BO}$) and non-bridging oxygen ($\frac{NBO}{NBO+BO}$) proportion as a function of the maximum pressure. The dots symbolize the extrapolation by the P1(full-colored) and P4 (empty) procedures. The horizontal lines mark these proportions for the average uncompressed population. The error bar due to the uncertainty propagation in the proportions is estimated as ±2% (not shown).

We propose that an increase in the proportion of NBO occurs at the expense of BO (Figure 5), leading to depolymerization as a function of maximum pressure. Such occurrence implies not only the existence of free oxygen (O^{2-}) within the uncompressed glass structure but also their consumption in the permanently densified glasses. Perhaps the saturation in structural changes at 20 GPa (Figure 3) is related to the complete consumption of O^{2-}.

Yoshimoto *et al.*[39] report an overall increase in the hardness and Young's modulus of densified lead silicate glasses with high PbO content, which these authors associated simultaneously with a strengthening, increasing covalency, of the Pb-O bonds and an increase in the number of bonds per unit volume. The lead coordination increase is consistent with their arguments, such that the pressure-induced increase in the NBO proportion is probably accompanied by the formation of highly coordinated Pb.

From their IR spectra for hot-densified lead silicate glass, Yoshimoto *et al.*[39] still reported modification of the Si-O stretching envelope, with a shift of the maximum towards lower frequencies, indicating also a possible silicon network depolymerization and overall NBO increase for the entire 33 to 67 mol.% PbO composition range. This last fact is contrary to the trend found in pressure-induced silicate glass with other compositions (e.g. sodium and aluminum), where the overall NBO population is generally reported to decrease with pressure [63, 69-71].

Direct measurements of BO, NBO and O^{2-} in permanently densified glass would be fundamental in order to test our hypothesis. To confirm the participation of lead cations in the compression mechanisms resulting in this unusual depolymerization, we plan to investigate in-situ the PS glass composition under pressure, probing the structural modifications on the short- and medium-range orders.

4. Conclusions

Ex-situ Raman measurements at room temperature were performed in lead metasilicate glass samples subjected to different maximum pressures. This enabled the determination of the elastic and saturation limits at 4 GPa and 20 GPa, respectively. The barycenter evolution of the high-frequency Raman envelope, attributed to Si-O stretching modes, displays a shift toward lower wavenumbers, which is we interpret as depolymerization with increasing pressure in $PbSiO_3$ glass. This conclusion was quantified with curve fitting modelling that gave a good estimation of the Q^n population and the evolution of the BO and NBO proportion as a function of the maximum pressure. While Q^2 fraction remains about the same, the Q^0 and Q^1 populations were found to increase slightly. With increasing pressure, $Q^{3'}$ was favored over Q^3 resulting in an overall decrease in the total Q^3. This interpretation is evidence of irreversible pressure-induced depolymerization of the silicate network after a compression/decompression cycle as shown by an increase in the NBO proportion. These results are in contrast to those reported for other silicate compositions, implying not only the existence but also consumption of free oxygen (O^{2-}) within the PS glass structure.

Acknowledgments

We are extremely thankful to Benjamin Moulton for his keen interest and remarks, and to the two anonymous reviewers for their constructive comments and most valuable insights, which resulted in a substantially improved manuscript. The authors are grateful to São Paulo Research Foundation (FAPESP) for funding this research through the CEPID project no. 2013/07793-6, the Brazilian grant no. 2017/11868-2 and Brazil-France cooperation grant no. 2019/11446-6. We are also thankful to CNRS-UCB Lyon 1 for their financial support. Raman experiments were performed at the vibrational spectroscopies Platform at University Lyon 1- France (CECOMO). High-pressure experiments were performed in the SOPRANO group at ILM laboratory at University Lyon 1.

References

1. Schoenung, J.M., *Lead Compounds*, in *Ceramic and Glass Materials: Structure, Properties and Processing*, J.F. Shackelford and R.H. Doremus, Editors. 2008, Springer US: Boston, MA. p. 151-167.
2. Singh, K.J., et al., *Gamma-ray shielding and structural properties of PbO–SiO_2 glasses.* Nuclear Instruments and Methods in Physics Research Section B: Beam Interactions with Materials and Atoms, 2008. **266**(6): p. 944-948.
3. Ruengsri, S., *Radiation Shielding Properties Comparison of Pb-Based Silicate, Borate, and Phosphate Glass Matrices.* Science and Technology of Nuclear Installations, 2014. **2014**: p. 218041.
4. Dayanand, C., G. Bhikshamaiah, and M. Salagram, *IR and optical properties of PbO glass containing a small amount of silica.* Materials Letters, 1995. **23**(4): p. 309-315.
5. Bair, G.J., *The Constitution of Lead Oxide-Silica Glasses: I, Atomic Arrangement.* Journal of the American Ceramic Society, 1936. **19**(1-12): p. 339-347.
6. Krogh-Moe, J., *An X-Ray Investigation of Lead Silicate Glass*, in *Zeitschrift für Physikalische Chemie*. 1958. p. 223.
7. Morikawa, H., Y. Takagi, and H. Ohno, *Structural analysis of 2PbO·SiO_2 glass.* Journal of Non-Crystalline Solids, 1982. **53**(1): p. 173-182.
8. Takagi, Y., et al., *X-ray Diffraction Analysis of the PbO–SiO_2 System in the Glassy and the Molten State.* Transactions of the Japan institute of metals, 1985. **26**(7): p. 451-461.
9. Imaoka, M., H. Hasegawa, and I. Yasui, *X-ray diffraction analysis on the structure of the glasses in the system PbO-SiO_2.* Journal of Non-Crystalline Solids, 1986. **85**(3): p. 393-412.
10. Takaishi, T., et al., *Structural Study on PbO–SiO_2 Glasses by X-Ray and Neutron Diffraction and ^{29}Si MAS NMR Measurements.* Journal of the American Ceramic Society, 2005. **88**(6): p. 1591-1596.
11. Kohara, S., et al., *Lead silicate glasses: Binary network-former glasses with large amounts of free volume.* Physical Review B, 2010. **82**(13): p. 134209.
12. Hagiwara, H. and R. Oyamada, *Raman Spectra of Glassy PbO-SiO_2 System.* Journal of the Physical Society of Japan, 1974. **36**(3): p. 917-917.
13. Worrell, C.A. and T. Henshall, *Vibrational spectroscopic studies of some lead silicate glasses.* Journal of Non-Crystalline Solids, 1978. **29**(3): p. 283-299.
14. Furukawa, T., S.A. Brawer, and W.B. White, *The structure of lead silicate glasses determined by vibrational spectroscopy.* Journal of Materials Science, 1978. **13**(2): p. 268-282.
15. Furukawa, T., S.A. Brawer, and W.B. White, *Raman and Infrared Spectroscopic Studies of the Crystalline Phases in the System Pb_2SiO_4-$PbSiO_3$.* Journal of the American Ceramic Society, 1979. **62**(7-8): p. 351-356.
16. Piriou, B. and H. Arashi, *Raman and Infrared Investigations of Lead Silicate-Glasses.* High Temperature Science, 1980. **13**(1-4): p. 299-313.
17. Ohno, H., et al., *Neutron irradiation effects of PbO-SiO_2 glasses.* Journal of Nuclear Materials, 1991. **179-181**: p. 473-476.
18. Feller, S., et al., *A multispectroscopic structural study of lead silicate glasses over an extended range of compositions.* Journal of Non-Crystalline Solids, 2010. **356**(6): p. 304-313.
19. Ben Kacem, I., et al., *Structure and properties of lead silicate glasses and melts.* Chemical Geology, 2017. **461**: p. 104-114.
20. Sampaio, D.V., et al., *Raman scattering and molecular dynamics investigation of lead metasilicate glass and supercooled liquid structures.* Journal of Non-Crystalline Solids, 2018. **499**: p. 300-308.
21. Liu, L., *Infrared spectroscopy on lead silicate glass.* Zeitschrift für Physik B Condensed Matter, 1993. **90**(4): p. 393-399.

22. De Sousa Meneses, D., M. Malki, and P. Echegut, *Structure and lattice dynamics of binary lead silicate glasses investigated by infrared spectroscopy.* Journal of Non-Crystalline Solids, 2006. **352**(8): p. 769-776.
23. Fayon, F., et al., *^{29}Si and ^{207}Pb NMR study of local order in lead silicate glasses.* Journal of Non-Crystalline Solids, 1998. **232-234**: p. 403-408.
24. Fayon, F., et al., *Pb^{2+} environment in lead silicate glasses probed by Pb-L_{III} edge XAFS and ^{207}Pb NMR.* Journal of Non-Crystalline Solids, 1999. **243**(1): p. 39-44.
25. Fujiu, T. and M. Ogino, *^{29}Si NMR study on the structure of lead-silicate glasses.* Journal of non-crystalline solids, 1984. **64**(1-2): p. 287-290.
26. Yoko, T., et al., *A ^{207}Pb MAS-NMR study of Pb-containing glasses.* Journal of Non-Crystalline Solids, 1992. **150**(1): p. 192-196.
27. Bessada, C., et al., *^{29}Si MAS-NMR in lead silicates.* Journal of Non-Crystalline Solids, 1994. **168**(1): p. 76-85.
28. Schneider, J., et al., *Q^n distribution in stoichiometric silicate glasses: thermodynamic calculations and ^{29}Si high resolution NMR measurements.* Journal of Non-Crystalline Solids, 2003. **325**(1): p. 164-178.
29. Lee, S.K. and E.J. Kim, *Probing metal-bridging oxygen and configurational disorder in amorphous lead silicates: insights from ^{17}O solid-state nuclear magnetic resonance.* The Journal of Physical Chemistry C, 2015. **119**(1): p. 748-756.
30. Cormier, G., T. Peres, and J.A. Capobianco, *Molecular dynamics simulation of the structure of undoped and Yb^{3+}-doped lead silicate glass.* Journal of Non-Crystalline Solids, 1996. **195**(1): p. 125-137.
31. Rybicki, J., et al., *Structure of lead-silicate glasses via constant-pressure MD simulations.* Computer Physics Communications, 1996. **97**(1): p. 191-194.
32. Rybicka, A., et al., *The structure of the first co-ordination shell of Pb atoms in lead-silicate glasses: a molecular dynamics study.* Computational Methods in Science and Technology, 1999. **5**: p. 67-74.
33. Rybicki, J., et al., *The structure of lead-silicate glasses: molecular dynamics and EXAFS studies.* Journal of Physics: Condensed Matter, 2001. **13**(43): p. 9781-9797.
34. Mastelaro, V.R., et al., *Relationship between short-range order and ease of nucleation in $Na_2Ca_2Si_3O_9$, $CaSiO_3$ and $PbSiO_3$ glasses.* Journal of Non-Crystalline Solids, 2000. **262**(1): p. 191-199.
35. Smets, B.M.J. and T.P.A. Lommen, *The structure of glasses and crystalline compounds in the system PbO-SiO_2, studied by X-ray photoelectron spectroscopy.* Journal of Non-Crystalline Solids, 1982. **48**(2): p. 423-430.
36. Wang, P.W. and L.P. Zhang, *Structural role of lead in lead silicate glasses derived from XPS spectra.* Journal of Non-Crystalline Solids, 1996. **194**(1-2): p. 129-134.
37. Dalby, K.N., et al., *Resolution of bridging oxygen signals from O 1s spectra of silicate glasses using XPS: Implications for O and Si speciation.* Geochimica et Cosmochimica Acta, 2007. **71**(17): p. 4297-4313.
38. Nesbitt, H.W., et al., *Direct and indirect evidence for free oxygen (O^{2-}) in MO-silicate glasses and melts (M = Mg, Ca, Pb).* American Mineralogist, 2015. **100**(11-12): p. 2566-2578.
39. Yoshimoto, M., et al., *Effects of densification on mechanical properties of lead silicate glasses.* Journal of the Ceramic Society of Japan, 1989. **97**(1132): p. 1446-1450.
40. Elliott, S.R., *Medium-range structural order in covalent amorphous solids.* Nature, 1991. **354**(6353): p. 445-452.
41. Pena, R.B., et al., *In-situ Raman spectroscopy unveils metastable crystallization in lead metasilicate glass.* Journal of Non-Crystalline Solids, 2020. **546**: p. 120254.
42. Cassar, D.R., et al., *Elemental and cooperative diffusion in a liquid, supercooled liquid and glass resolved.* The Journal of Chemical Physics, 2017. **147**(1): p. 014501.

43. Felipe Lancelotti, R., et al., *Is the structural relaxation of glasses controlled by equilibrium shear viscosity?* Journal of the American Ceramic Society, 2020. **104**: p. 2066-2076.
44. Klotz, S., et al., *Hydrostatic limits of 11 pressure transmitting media.* Journal of Physics D: Applied Physics, 2009. **42**(7): p. 075413.
45. Mao, H.K., J. Xu, and P.M. Bell, *Calibration of the ruby pressure gauge to 800 kbar under quasi-hydrostatic conditions.* Journal of Geophysical Research: Solid Earth, 1986. **91**(B5): p. 4673-4676.
46. Deschamps, T., et al., *Elastic anomalous behavior of silica glass under high-pressure: In-situ Raman study.* Journal of Non-Crystalline Solids, 2009. **355**(18): p. 1095-1098.
47. Moulton, B.J.A., et al., *In situ structural changes of amorphous diopside ($CaMgSi_2O_6$) up to 20 GPa: A Raman and O K-edge X-ray Raman spectroscopic study.* Geochimica et Cosmochimica Acta, 2016. **178**: p. 41-61.
48. Rouxel, T., et al., *Poisson's Ratio and the Densification of Glass under High Pressure.* Physical Review Letters, 2008. **100**(22): p. 225501.
49. Mackenzie, J.D., *High-Pressure Effects on Oxide Glasses: I, Densification in Rigid State.* Journal of the American Ceramic Society, 1963. **46**(10): p. 461-470.
50. Huang, L. and J. Kieffer, *Amorphous-amorphous transitions in silica glass. II. Irreversible transitions and densification limit.* Physical Review B, 2004. **69**(22): p. 224204.
51. Poe, B.T., C. Romano, and G. Henderson, *Raman and XANES spectroscopy of permanently densified vitreous silica.* Journal of Non-Crystalline Solids, 2004. **341**(1): p. 162-169.
52. Salmon, P.S. and A. Zeidler, *Networks under pressure: the development of in-situ high-pressure neutron diffraction for glassy and liquid materials.* Journal of Physics: Condensed Matter, 2015. **27**(13): p. 133201.
53. Deschamps, T., et al., *Elastic Moduli of Permanently Densified Silica Glasses.* Scientific Reports, 2014. **4**(1): p. 7193.
54. Deschamps, T., et al., *Soda-lime silicate glass under hydrostatic pressure and indentation: a micro-Raman study.* Journal of Physics: Condensed Matter, 2011. **23**(3): p. 035402.
55. Meade, C. and R. Jeanloz, *Frequency-dependent equation of state of fused silica to 10 GPa.* Physical Review B, 1987. **35**(1): p. 236-244.
56. Lee, S.K., et al., *Degree of Permanent Densification in Oxide Glasses upon Extreme Compression up to 24 GPa at Room Temperature.* The Journal of Physical Chemistry Letters, 2020: p. 2917-2924.
57. Meade, C., R.J. Hemley, and H.K. Mao, *High-pressure x-ray diffraction of SiO_2 glass.* Physical Review Letters, 1992. **69**(9): p. 1387-1390.
58. Williams, Q. and R. Jeanloz, *Spectroscopic Evidence for Pressure-Induced Coordination Changes in Silicate Glasses and Melts.* Science, 1988. **239**(4842): p. 902.
59. Lin, J.F., et al., *Electronic bonding transition in compressed SiO_2 glass.* Physical Review B, 2007. **75**(1): p. 012201.
60. Sato, T. and N. Funamori, *High-pressure structural transformation of SiO_2 glass up to 100 GPa.* Physical Review B, 2010. **82**(18): p. 184102.
61. Benmore, C.J., et al., *Structural and topological changes in silica glass at pressure.* Physical Review B, 2010. **81**(5): p. 054105.
62. Susman, S., et al., *Intermediate-range order in permanently densified vitreous SiO_2: A neutron-diffraction and molecular-dynamics study.* Physical Review B, 1991. **43**(1): p. 1194.
63. Xue, X., et al., *Pressure-induced silicon coordination and tetrahedral structural changes in alkali oxide-silica melts up to 12 GPa: NMR, Raman, and infrared spectroscopy.* American Mineralogist, 1991. **76**(1-2): p. 8-26.
64. Wolf, G.H., D.J. Durben, and P.F. McMillan, *High-pressure Raman spectroscopic study of sodium tetrasilicate ($Na_2Si_4O_9$) glass.* The Journal of Chemical Physics, 1990. **93**(4): p. 2280-2288.

65. Dickinson Jr, J.E., C.M. Scarfe, and P. McMillan, *Physical properties and structure of $K_2Si_4O_9$ melt quenched from pressures up to 2.4 GPa.* Journal of Geophysical Research: Solid Earth, 1990. **95**(B10): p. 15675-15681.
66. Kubicki, J.D., R.J. Hemley, and A.M. Hofmeister, *Raman and infrared study of pressure-induced structural changes in $MgSiO_3$, $CaMgSi_2O_6$, and $CaSiO_3$ glasses.* American Mineralogist, 1992. **77**(3-4): p. 258-269.
67. Gaudio, S.J., S. Sen, and C.E. Lesher, *Pressure-induced structural changes and densification of vitreous $MgSiO_3$.* Geochimica et Cosmochimica Acta, 2008. **72**(4): p. 1222-1230.
68. Moulton, B.J.A., et al., *Structure—longitudinal sound velocity relationships in glassy anorthite ($CaAl_2Si2O8$) up to 20 GPa: An in situ Raman and Brillouin spectroscopy study.* Geochimica et Cosmochimica Acta, 2019. **261**: p. 132-144.
69. Stebbins, J.F., J. Wu, and L.M. Thompson, *Interactions between network cation coordination and non-bridging oxygen abundance in oxide glasses and melts: Insights from NMR spectroscopy.* Chemical Geology, 2013. **346**: p. 34-46.
70. Lee, S.K., et al., *Nature of polymerization and properties of silicate melts and glasses at high pressure.* Geochimica et Cosmochimica Acta, 2004. **68**(20): p. 4189-4200.
71. Allwardt, J.R., B.C. Schmidt, and J.F. Stebbins, *Structural mechanisms of compression and decompression in high-pressure $K_2Si_4O_9$ glasses: an investigation utilizing Raman and NMR spectroscopy of glasses and crystalline materials.* Chemical Geology, 2004. **213**(1): p. 137-151.
72. Bancroft, G.M., et al., *Lorentzian dominated lineshapes and linewidths for Raman symmetric stretch peaks (800–1200 cm^{-1}) in Q^n (n = 1–3) species of alkali silicate glasses/melts.* Journal of Non-Crystalline Solids, 2018. **484**: p. 72-83.
73. Nesbitt, H.W., et al., *Factors affecting line shapes and intensities of Q^3 and Q^4 Raman bands of Cs silicate glasses.* Chemical Geology, 2019. **505**: p. 1-11.
74. O'Shaughnessy, C., et al., *The influence of modifier cations on the Raman stretching modes of Q^n species in alkali silicate glasses.* Journal of the American Ceramic Society, 2020. **103**(7): p. 3991-4001.
75. Nesbitt, H.W., et al., *Bridging, non-bridging and free (O^{2-}) oxygen in Na_2O-SiO_2 glasses: An X-ray Photoelectron Spectroscopic (XPS) and Nuclear Magnetic Resonance (NMR) study.* Journal of Non-Crystalline Solids, 2011. **357**(1): p. 170-180.